Diosgenin derivatives developed from Pd(II) catalysed dehydrogenative coupling exert effect on breast cancer cells by abrogating growth and facilitating apoptosis via regulating AKT1 pathway

Supplementary information

Experimental details

Oven dried clean glass wares and organic reagents purchased from commercial chemical vendors were used and were dried according to the standard procedure.[S1] Potassium tetrachloropalladate(II) $K_2[PdCl_4]$ was prepared as reported elsewhere.[S2] The ligands 4-oxo-4*H*-chromene-3-carbaldehyde-4(*N*)-substituted thiosemicarbazones were prepared as reported by our group earlier.[S3] Melting points were determined by using a RAAGA apparatus. Elemental analyses were measured by using Vario EL III CHNS analyzer. FT-IR spectra were recorded with JASCO FT-IR 4100 instrument between 400 and 4000 cm^{-1} as KBr pellets. Electronic spectra were run on a JASCO V-630 spectrophotometer, using DMSO as a solvent in 200-800 nm range. ^1H NMR spectra were recorded at room temperature in $CDCl_3$ and DMSO-d_6 by using a Bruker 400 MHz instrument. Chemical shifts (δ) were presented in parts per million (ppm) with reference to tetramethylsilane (TMS). The mass spectra of the complexes and diosgenin coupled products were recorded using LCMS-2010A SHIMADZU instrument.

Results and discussion

IR Spectroscopy

Formation of ligands and their metal complexes was preliminarily confirmed by using IR spectroscopy. A very strong band in the IR spectra of the ligands around ~1533-1598 cm^{-1} corresponding to azomethine group,[S3,S4] was shifted to 1545-1550 cm^{-1} upon complexation with Pd(II) ion, confirming the involvement of azomethine nitrogen in coordination.[S3,S4] A characteristic absorption band around 1627-1641 cm^{-1} in the ligands was due to $\nu_{C=O}$ (ring carbonyl) vibration.[S3,S5] In the complexes, the $\nu_{C=O}$ vibration was observed around 1611-1612 cm^{-1}, which demonstrated the coordination of ketonic oxygen of chromone to palladium ion.[S3,S5] A band assignable to C=S of the ligands was present at 844-850 cm^{-1}, disappeared in the spectra of the complexes and a new band appeared at 752-760 cm^{-1} indicating the C-S coordination of sulfur atom after enolization and subsequent deprotonation.[S6]

Electronic spectroscopy

The electronic spectra of the complexes recorded in DMSO showed five bands in the regions of 216-262, 282-317, 399-408, 422-429 and 445-456 nm in the UV-Visible spectra (Figure S1). The bands around 216-262 and 282-317 nm corresponding to intra ligand transitions and the bands at 399-408 and 422-456 nm were due to the metal to ligand charge transfer (MLCT) transitions which are similar to the reported square planar palladium(II) complexes.[S5,S7-S10]

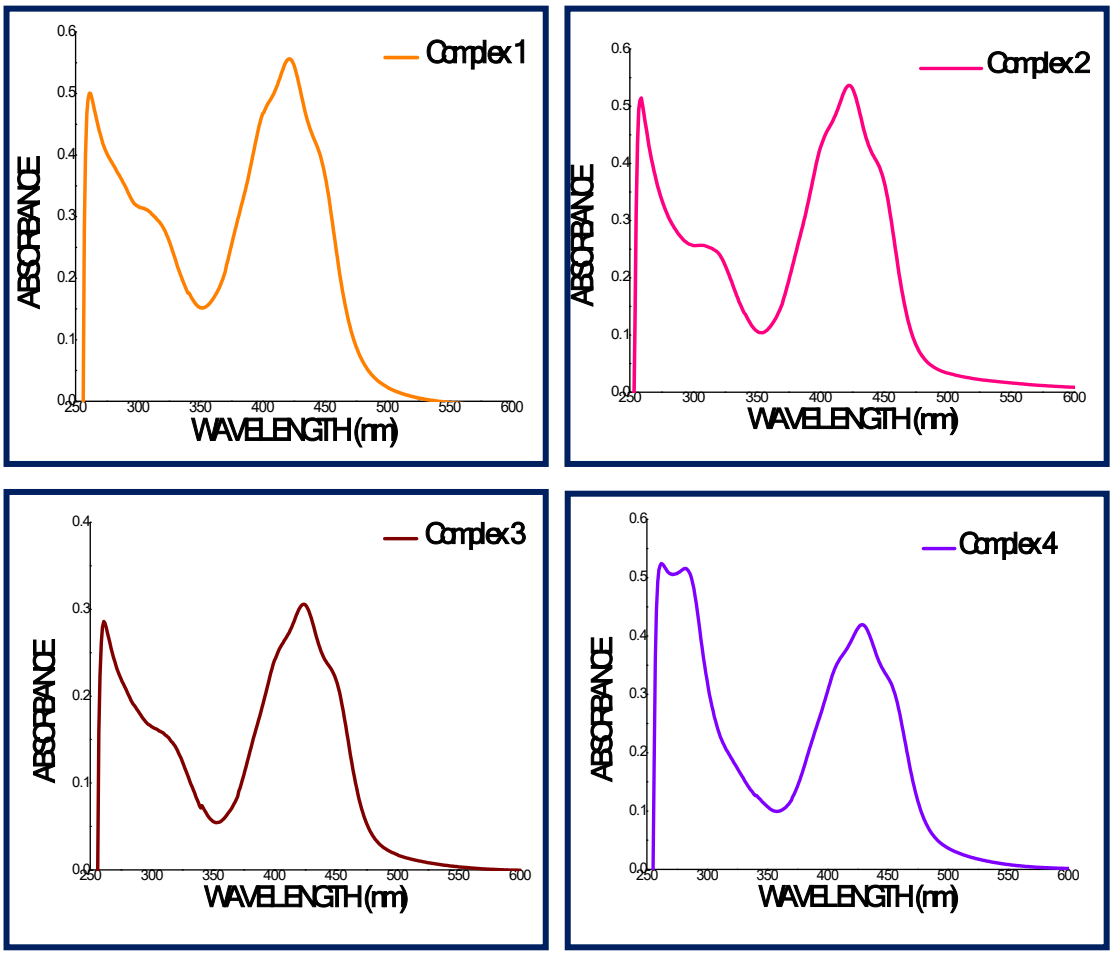

Fig. S1. UV-Visible spectra of the Pd(II) complexes (C1-C4)

^{1}H NMR spectroscopy

^{1}H NMR spectra of the ligands 4-oxo-4*H*-chromene-3-carbaldehyde-4(*N*)-substituted thiosemicarbazones,[S11] were compared with the complexes recorded in DMSO-d^{6} at room temperature (Figure S2-S5). N(2)-H proton of the ligands at δ 11.52-11.93 ppm completely disappeared in the complexes indicating the coordination of sulfur atom after deprotonation i.e.

in thiolate form.[S3,S5,S12] Complex **[Pd(FC-tsc)Cl]** (**C1**) showed a singlet at δ 7.25 ppm owing to the NH_2 protons. Terminal –NH protons of the complexes [**Pd(FC-mtsc)Cl]** (**C2**), [**Pd(FC-etsc)Cl]** (**C3**) and [**Pd(FC-ptsc)Cl]** (**C4**) were observed as singlets at δ 7.66, 7.72 and 9.94 ppm respectively.[S13] The spectrum of the complex [**Pd(FC-mtsc)Cl]** (**C2**) showed a doublet at δ 2.78-2.80 ppm for methyl protons. For the complex [**Pd(FC-etsc)Cl]** (**C3**), the signal for methyl protons has been observed as a triplet at δ 1.08-1.12 ppm. Further, a multiplet at δ 3.17-3.24 ppm was assigned to the methylene protons of **[Pd(FC-etsc)Cl]** (**C3**).[S6,S13]

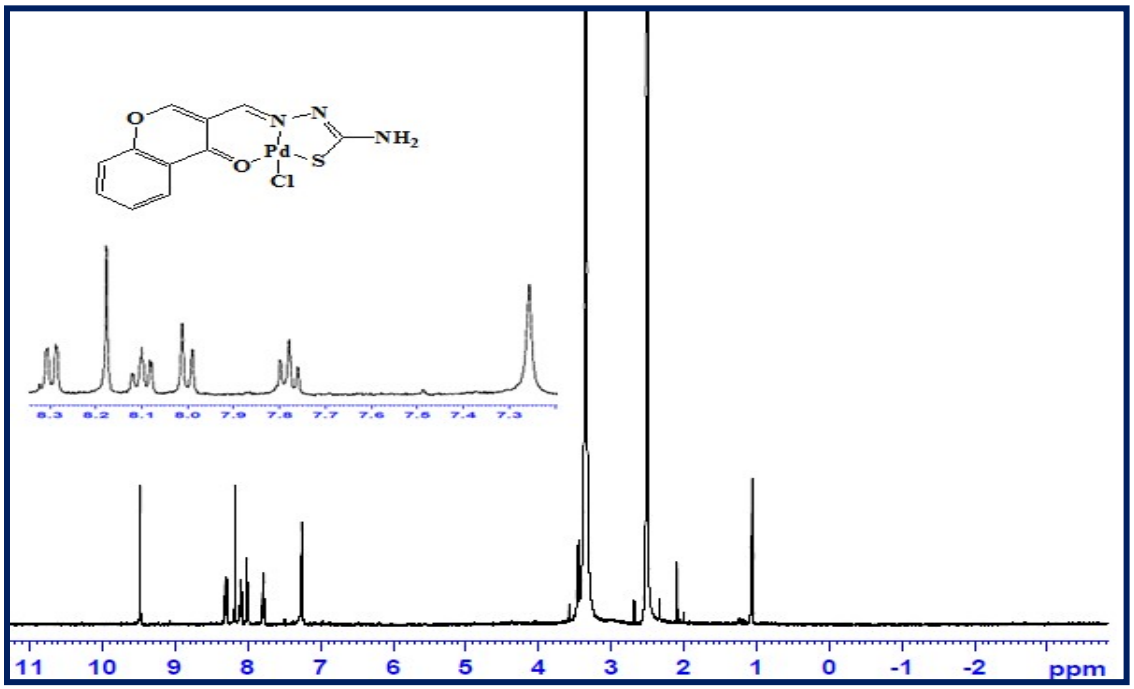

Fig. S2. ^{1}H NMR spectrum of complex [Pd(FC-tsc)Cl] (C1)

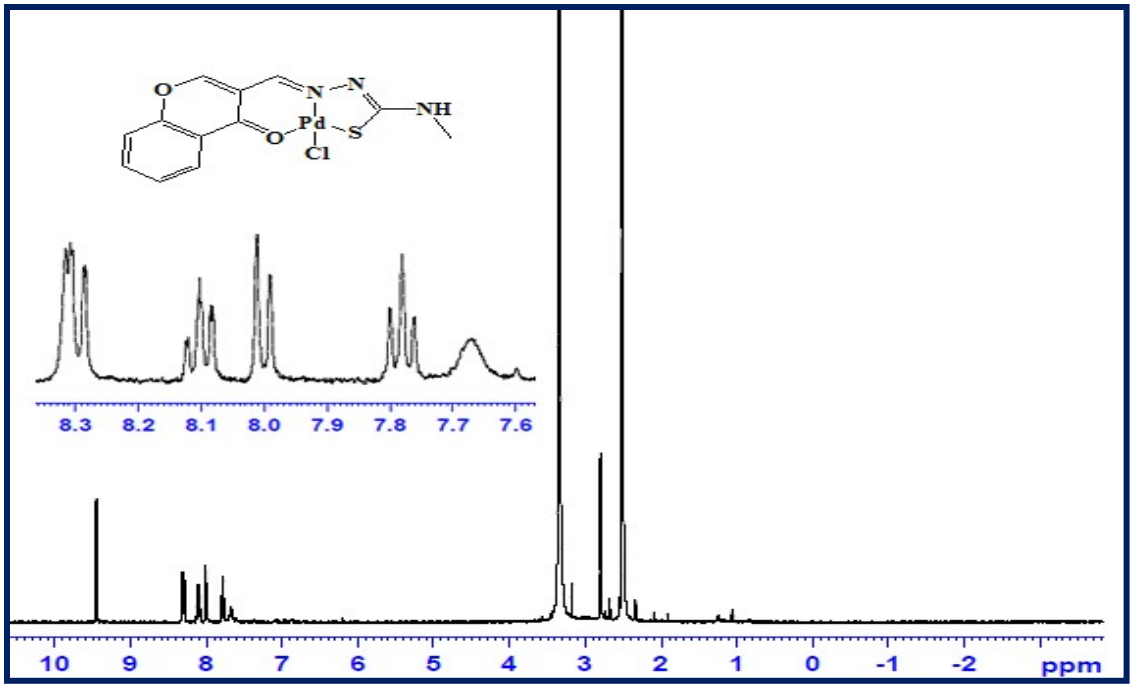

Fig. S3. ^{1}H NMR spectrum of complex [Pd(FC-mtsc)Cl] (C2)

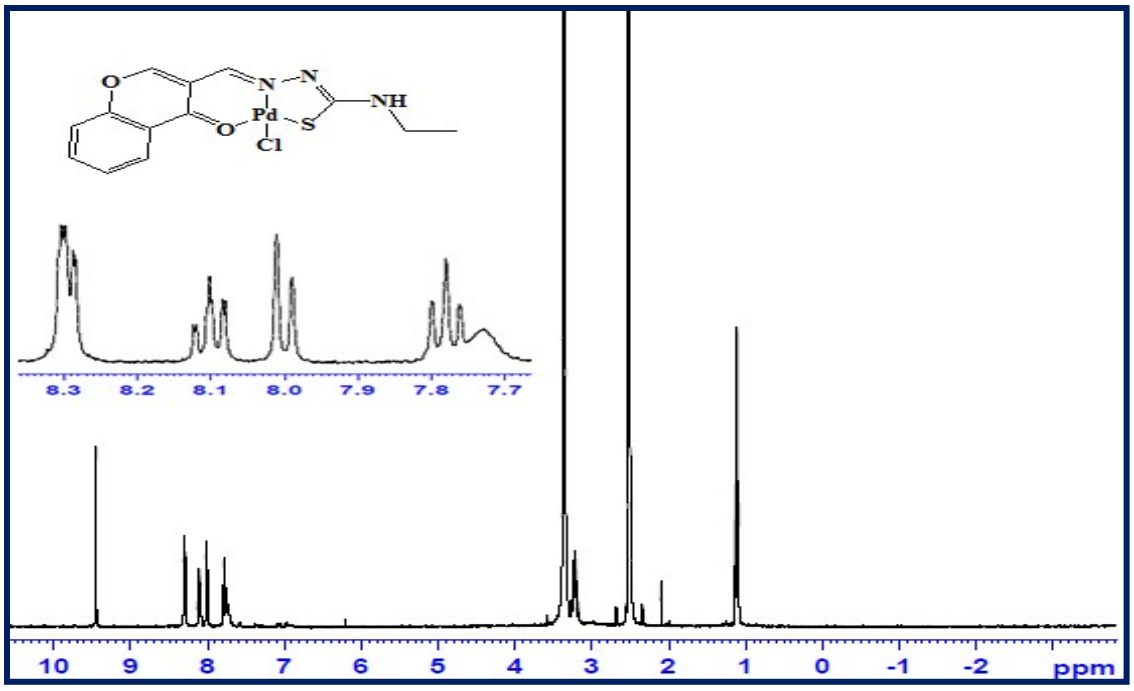

Fig. S4. ^{1}H NMR spectrum of complex [Pd(FC-etsc)Cl] (C3)

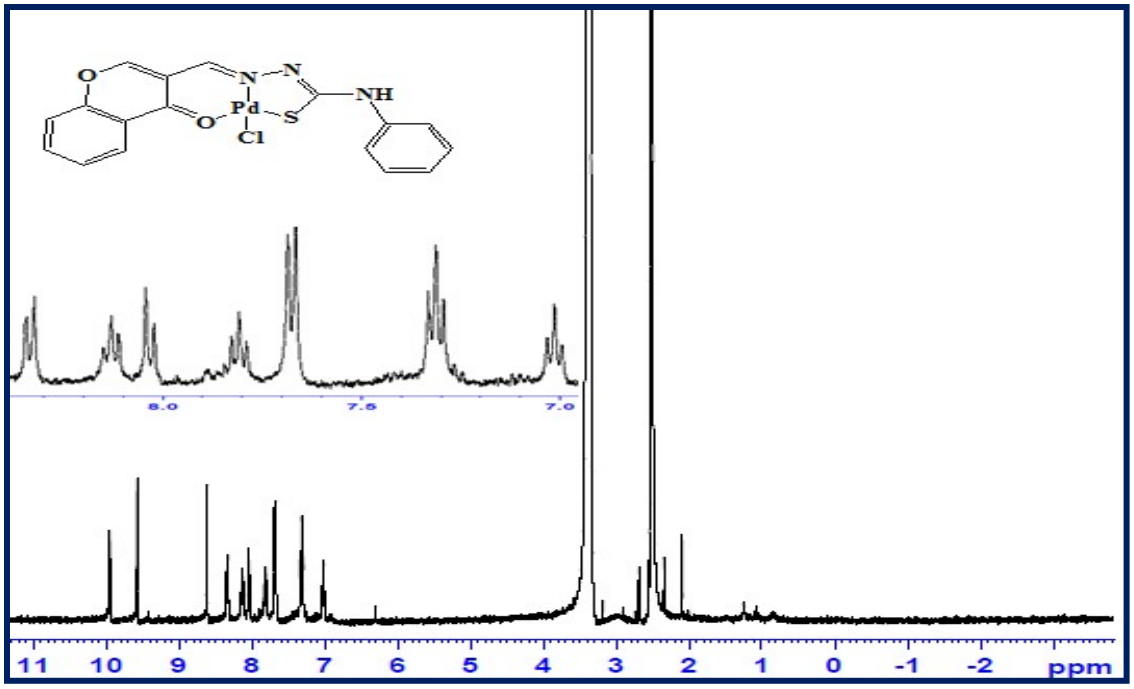

Fig. S5. ^{1}H NMR spectrum of complex [Pd(FC-ptsc)Cl] (C4)

Mass spectral analysis

Mass spectra were recorded for all the complexes to support their molecular stoichiometry. They showed molecular ion peaks corresponding to $[M+H]^+$ at 389.35 ([**Pd(FC-tsc)Cl**] (**C1**)), 403.30 ([**Pd(FC-mtsc)Cl**] (**C2**)), 417.35 ([**Pd(FC-etsc)Cl**] (**C3**)) and 465.30 ([**Pd(FC-ptsc)Cl**] (**C4**)) respectively (Fig. S6-S9).

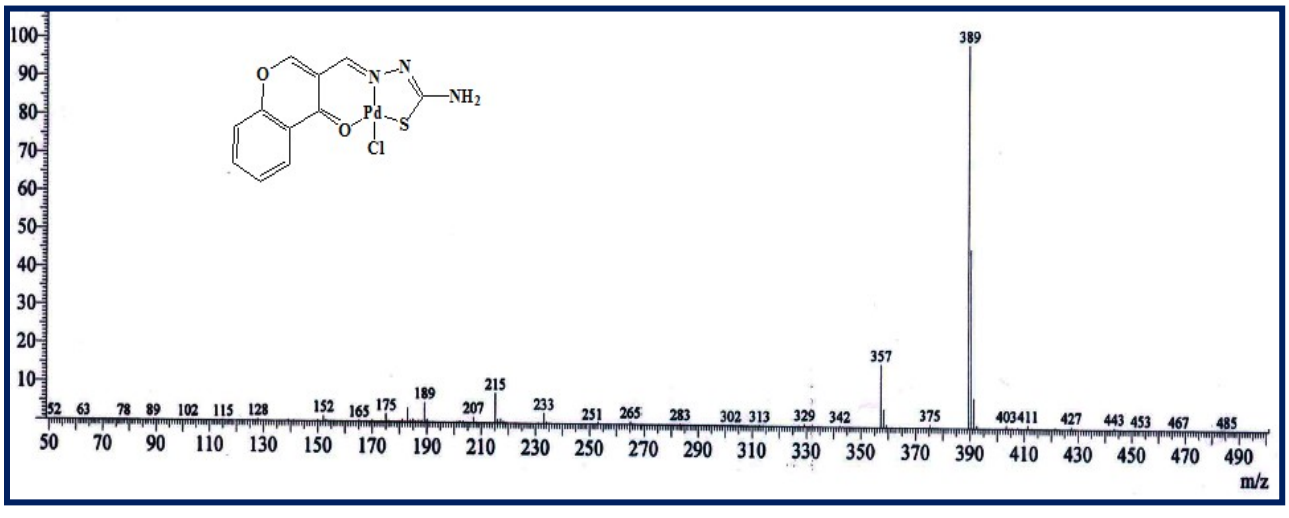

Fig. S6. LCMS spectrum of complex [Pd(FC-tsc)Cl] (C1)

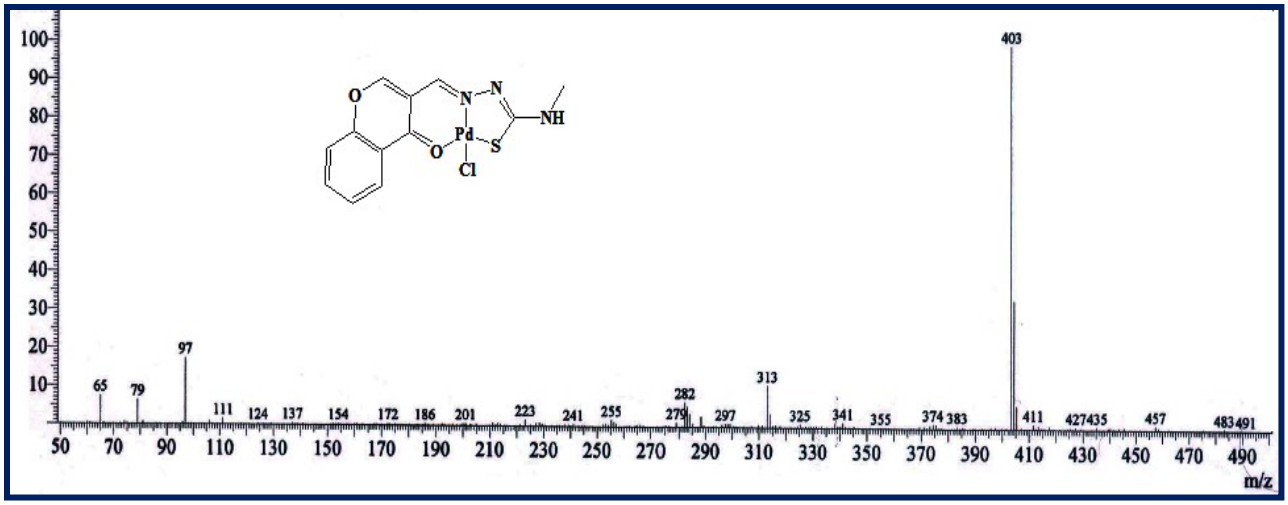

Fig. S7. LCMS spectrum of complex [Pd(FC-mtsc)Cl] (C2)

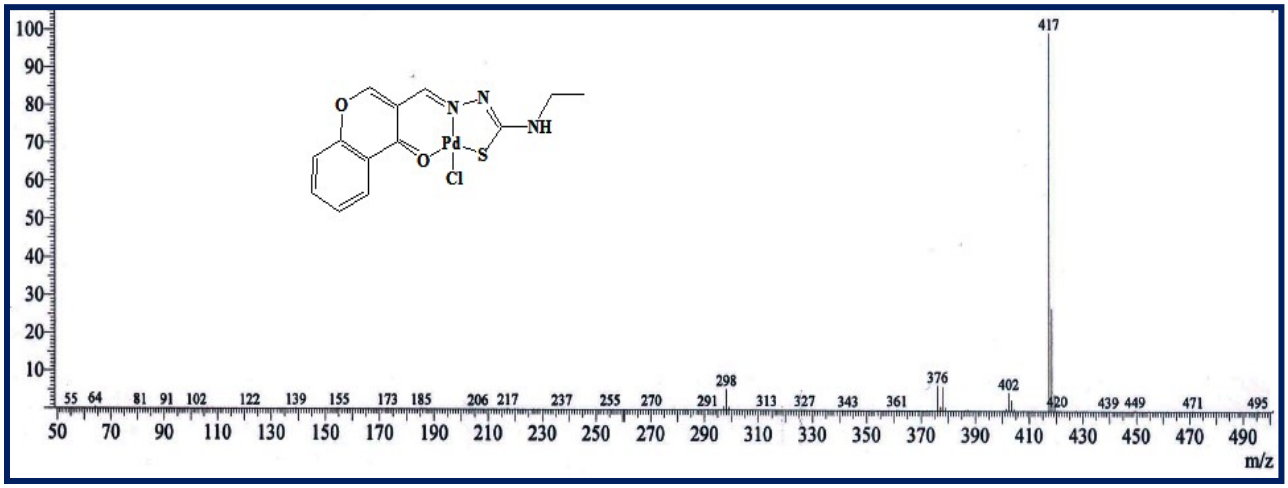

Fig. S8. LCMS spectrum of complex [Pd(FC-etsc)Cl] (C3)

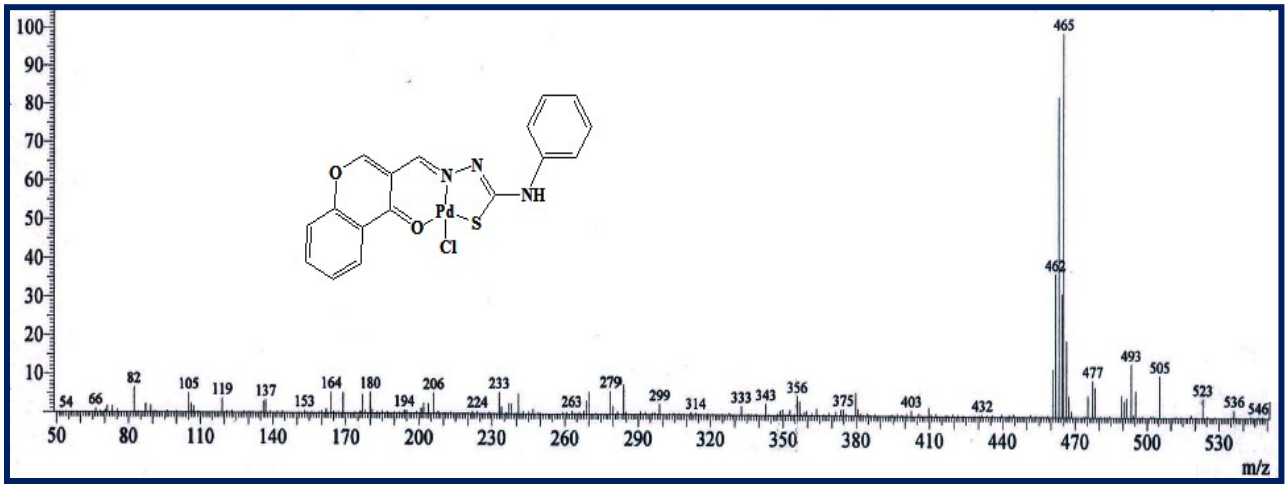

Fig. S9. LCMS spectrum of complex [Pd(FC-ptsc)Cl] (C4)

X-ray crystallography

Solid state structure of complex C1

Complex [**Pd(FC-tsc)Cl] (C1)** has been structurally characterized by X-ray diffraction analysis (Fig. 1; Table S1 and S2). It belongs to triclinic crystal system with P -1 space group. There is one DMF and water molecule in the crystal lattice came through the solvent of crystallisation. The ligand [**H-FC-tsc]** exhibited mononegative tridentate ONS coordination to the palladium ion, with Pd1-O1, Pd1-N1 and Pd1-S1 bond distances of 2.0695 (16), 1.9848 (19) and 2.2266 (7) Å respectively which were found to be similar with the reported palladium(II) square planar complexes [S14-S16]. A chloride ion occupied the fourth coordination site, thereby satisfying the +2 charge of the palladium ion. The metal ion with the coordinated ligand adopted a distorted square planar geometry having *cis* angles N1-Pd1-O1 (93°) and N1-Pd1-S1 (85°) and *trans* angles O1-Pd1-S1 (178°) and N1-Pd1-Cl1 (175°) which deviated significantly from ideal *cis* and *trans* angle.

Table S1. Crystal data and structure refinement for the complex **C1**

	[Pd(FC-tsc)Cl].DMF.H_2O (C1)	
Empirical formula	$C_{14}H_{17}Cl\ N_4O_4PdS$	
Formula weight	479.22	
Temperature	100(2) K	
Wavelength	0.71073 Å	
Crystal system	triclinic	
Space group	P -1	
Unit cell dimensions	a = 7.3080(19) Å	α = 88.662(6)°
	b = 9.042(2) Å	β = 82.640(5)°
	c = 13.221(3) Å	γ = 86.314(6)°
Volume	864.6(4) $Å^3$	
Z	2	
Density	1.841 Mg/m^3	
Absorption coefficient	1.376 mm^{-1}	
F(000)	480	
Crystal size	0.38 x 0.31 x 0.30 mm^3	
Theta range for data collection	2.760 to 28.400°.	
Index ranges	-9≤h≤9, -12≤k≤12, -17≤l≤17	
Reflections collected	11272	
Independent reflections	4261 [R(int) = 0.0439]	

Completeness to theta = 25.242°	99.8 %
Absorption correction	Numerical
Max. and min. transmission	0.7983 and 0.6979
Refinement method	Full-matrix least-squares on F^2
Data/ restraints/ parameters	4261/ 338/ 291
Goodness-of-fit on F^2	1.026
Final R indices [I>2σ(I)]	R1 = 0.0280, wR2 = 0.0627
R indices (all data)	R1 = 0.0334, wR2 = 0.0657

Table S2. Selected bond lengths (Å) and angles (°) of complex **C1**

[Pd(FC-tsc)Cl].DMF.H_2O (C1)	
Pd(1)-N(1)	1.9848(19)
Pd(1)-O(1)	2.0695(16)
Pd(1)-S(1)	2.2266(7)
Pd(1)-Cl(1)	2.3191(7)
Bond angles	
[Pd(FC-tsc)Cl].DMF.H_2O (C1)	
N1-Pd1-O1	93.49(7)
N1-Pd1-S1	85.05(6)
O1-Pd1-S1	178.21(5)
N1-Pd1-Cl1	175.81(6)
O1-Pd1-Cl1	90.67(5)
S1-Pd1-Cl1	90.80(3)

Hydrogen bonding interactions

There are four hydrogen bonding interactions were found in the complex **[Pd(FC-tsc)Cl]** (**C1**) - i) N2 atom of one molecule is intermolecularly hydrogen bonded with H3B(N3) of adjacent molecule, ii) H3A(N3) of one molecule showed hydrogen bonding to O3 atom of water molecule, iii) H3B(N3) of first molecule is hydrogen bonded to N2 atom of second molecule and iv) Cl1 atom of one molecule is hydrogen bonded to H3D(O3) of water molecule. These hydrogen bonding interactions gave a sheet like structure (Fig. S10; Table S3).

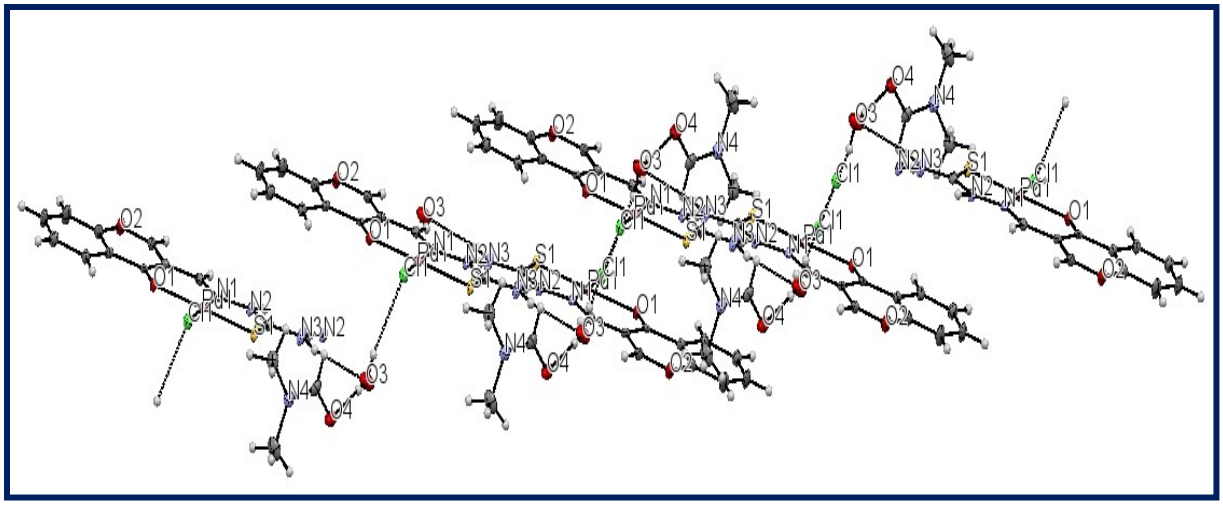

Fig. S10. ORTEP diagram of the complex **C1** with hydrogen bondings

Table S3. Hydrogen bonds for complex **C1** [Å and °]

D-H...A	d(D-H)	d(H...A)	d(D...A)	<(DHA)
O3-H3C...O4	0.69(3)	2.02(3)	2.706(5)	175(4)
O3-H3C...O4A	0.69(3)	2.19(3)	2.867(5)	166(4)
O3-H3D...Cl1#1	0.78(4)	2.44(4)	3.208(3)	166(3)
N3-H3A...O3	0.84(3)	2.31(3)	3.076(3)	151(2)
N3-H3B...N2#2	0.87(3)	2.16(4)	3.021(3)	173(3)

Symmetry transformations used to generate equivalent atoms:
#1 x,y+1,z #2 -x,-y+2,-z+1

Catalytic application of the Pd(II) complexes C1-C4

Optimization of reaction conditions

Table S4. Optimization of reaction conditions

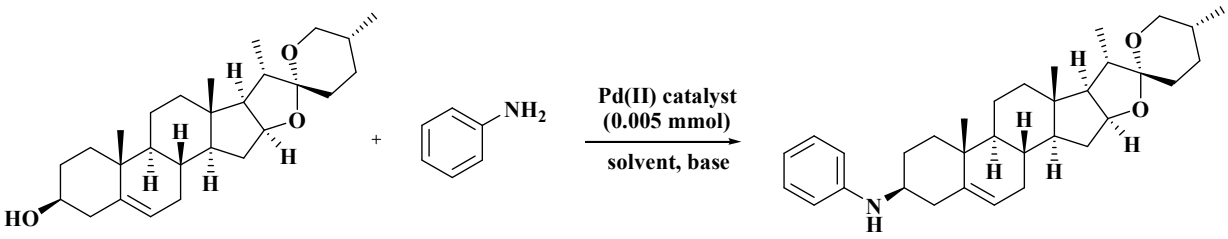

Entry	Solvent	Base (mmol)	Complex (0.005 mmol)	Temperature (^oC)	Time (h)	Yield (%)[a]
1	EtOH	KOH (1.5)	**C1**	rt	4	61
2	**MeOH**	**KOH (1.5)**	**C1**	**rt**	**4**	**65**
3	CH_3CN	KOH (1.5)	**C1**	rt	4	56
4	DMF	KOH (1.5)	**C1**	rt	4	55
5	DMSO	KOH (1.5)	**C1**	rt	4	48
6	$CHCl_3$	KOH (1.5)	**C1**	rt	4	21
7	DCM	KOH (1.5)	**C1**	rt	4	33
8	Benzene	KOH (1.5)	**C1**	rt	4	59
9	Toluene	KOH (1.5)	**C1**	rt	4	53
10	Dioxane	KOH (1.5)	**C1**	rt	4	56
11	2-methoxyethanol	KOH (1.5)	**C1**	rt	4	38
12	Isopropanol	KOH (1.5)	**C1**	rt	4	36
13	MeOH	KOH (1.5)	**C1**	50	4	15
14	MeOH	KOH (1.5)	**C1**	60	4	23
15	MeOH	KOH (1.5)	**C1**	reflux	4	39
16	MeOH	KOH (1.5)	**C2**	rt	4	53
17	MeOH	KOH (1.5)	**C3**	rt	4	59
18	MeOH	KOH (1.5)	**C4**	rt	4	61

Reaction conditions: Diosgenin (1 mmol), amine (1 mmol), base (1.5 mmol), catalyst (0.005 mmol). rt - room temperature. [a]Isolated yield.

Table S5. Optimization by varying base

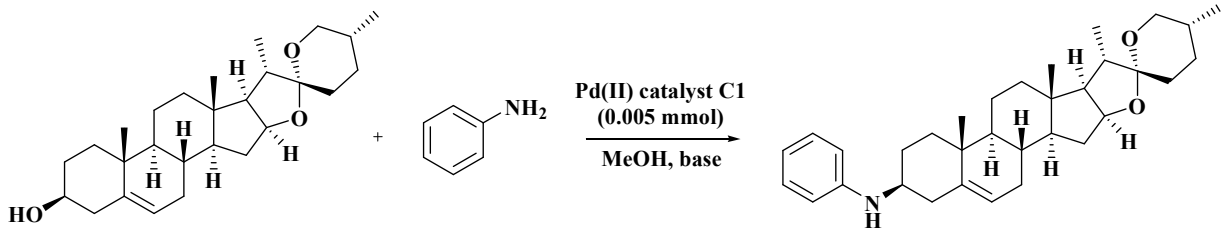

Entry	Base (mmol)	Catalyst (mmol)	Temperature	Time (h)	Yield (%)[a]
1	KOH (1.5)	0.005	rt	4	65
2	NaOH (1.5)	0.005	rt	4	61
3	K_2CO_3 (1.5)	0.005	rt	4	55
4	Na_2CO_3 (1.5)	0.005	rt	4	46
5	Cs_2CO_3 (1.5)	0.005	rt	4	37
6	Et_3N (1.5)	0.005	rt	4	43
7	KOH (1.5)	**No catalyst**	rt	4	NR
8	**No base**	**0.005**	**rt**	**4**	**65**

Reaction conditions: Diosgenin (1 mmol), amine (1 mmol). rt - room temperature. [a]Isolated yield. NR - No reaction

LCMS data for representative coupled products

D7: 453.300 $[0.5M.CH_3CN]^+$

D8: 852.950 $[M]^+$

D10: 901.200 $[M]^+$

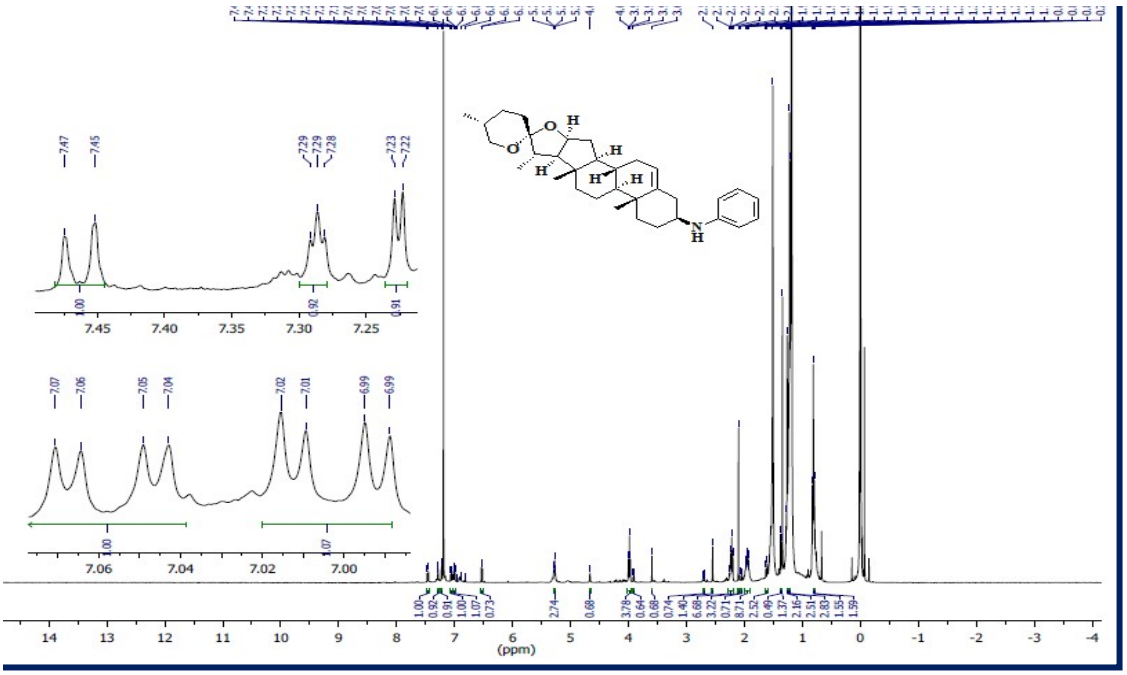

Fig. S11. ^{1}H NMR spectrum of **D1**

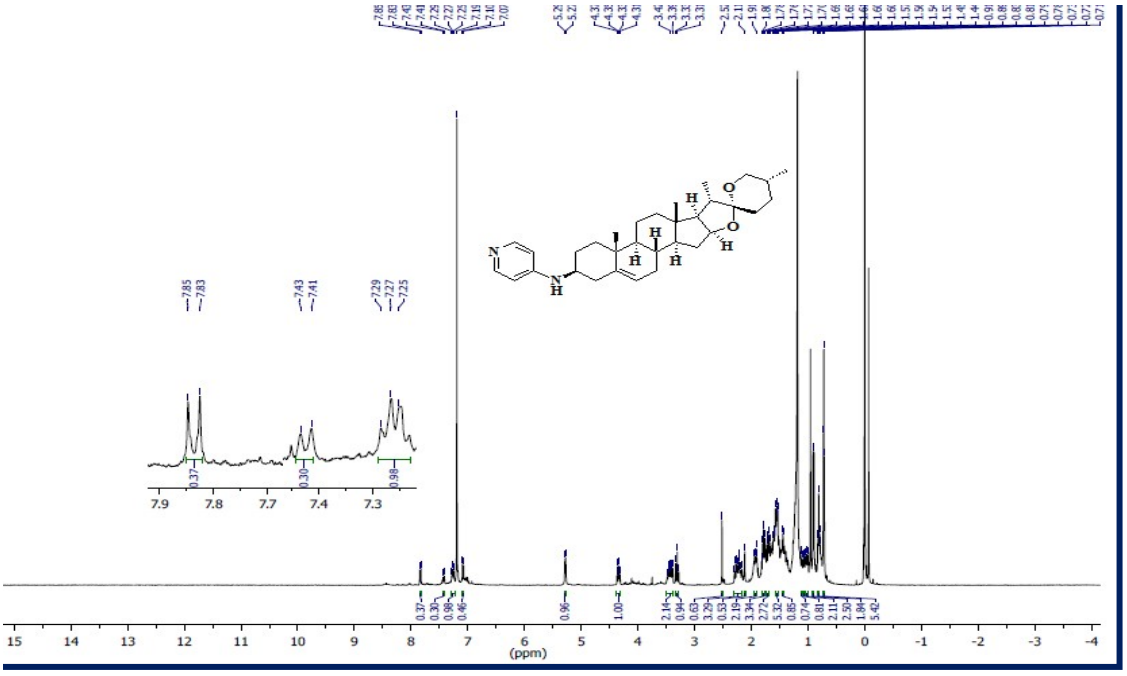

Fig. S12. ^{1}H NMR spectrum of **D2**

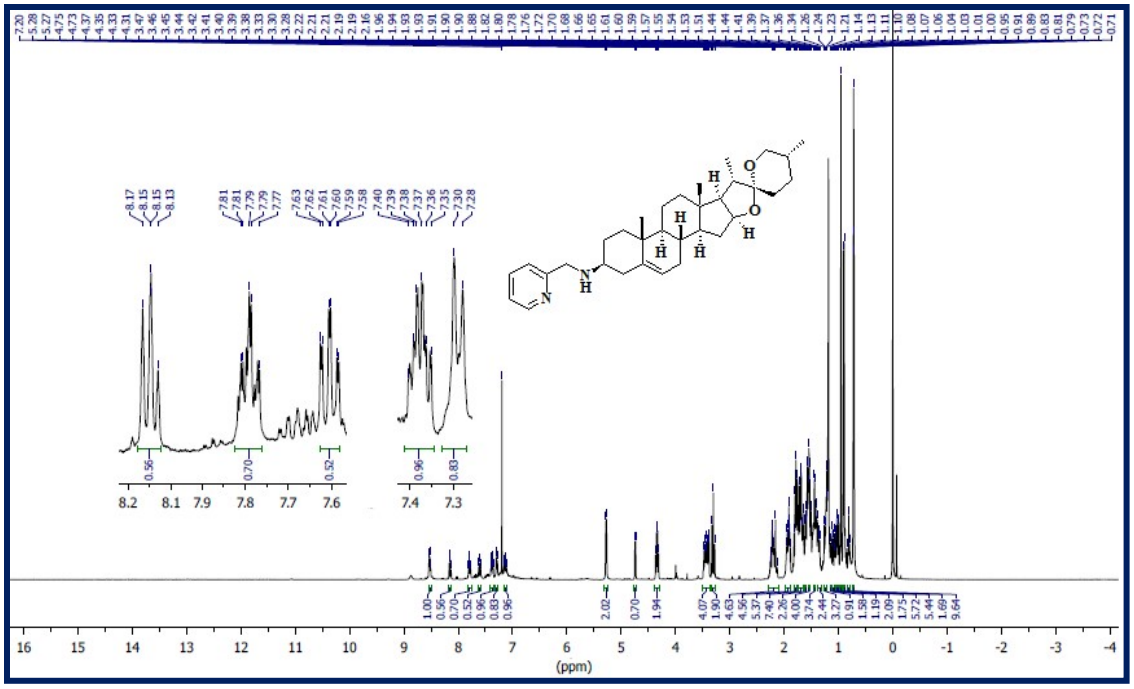

Fig. S13. ^{1}H NMR spectrum of **D3**

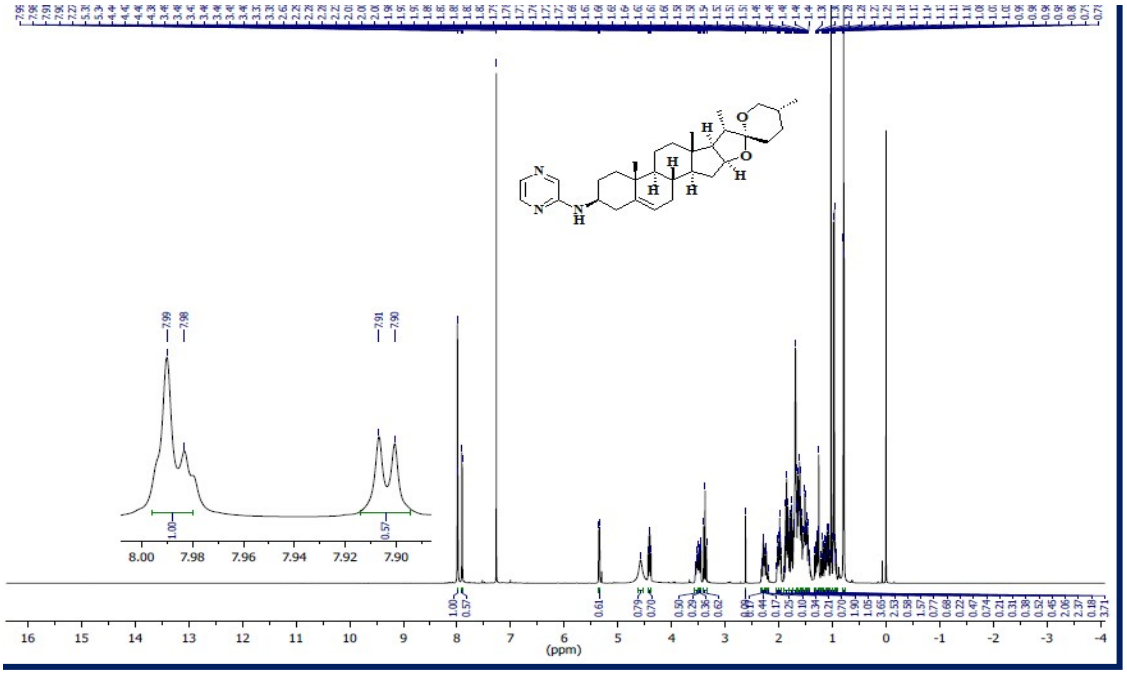

Fig. S14. ^{1}H NMR spectrum of **D4**

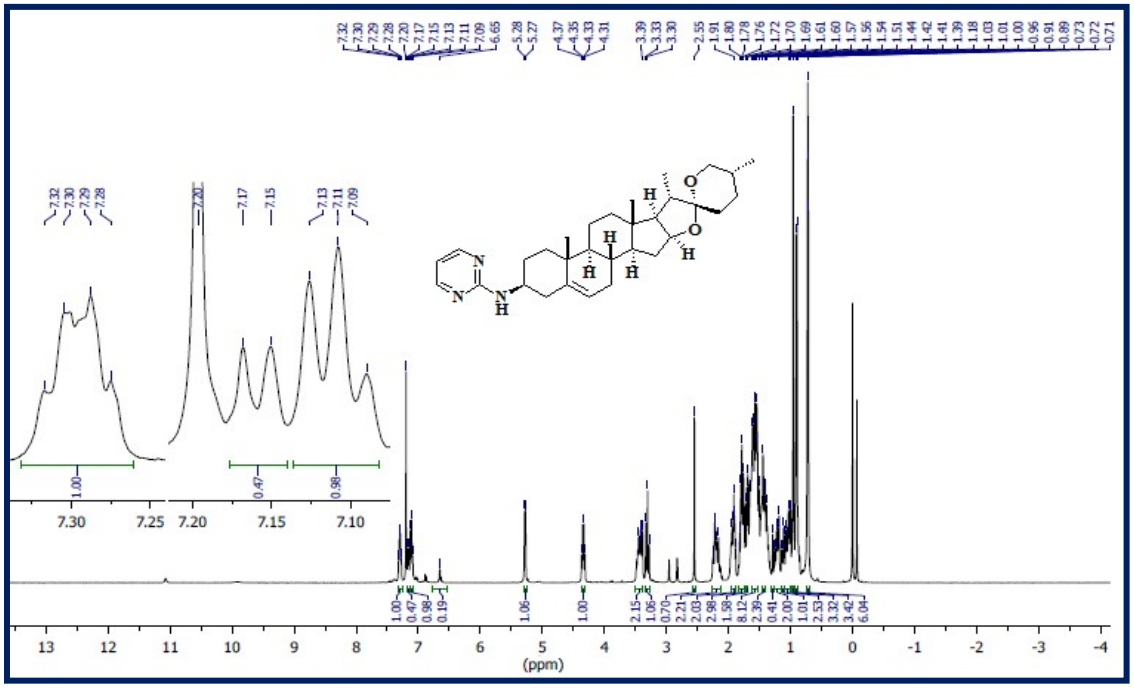

Fig. S15. ^{1}H NMR spectrum of **D5**

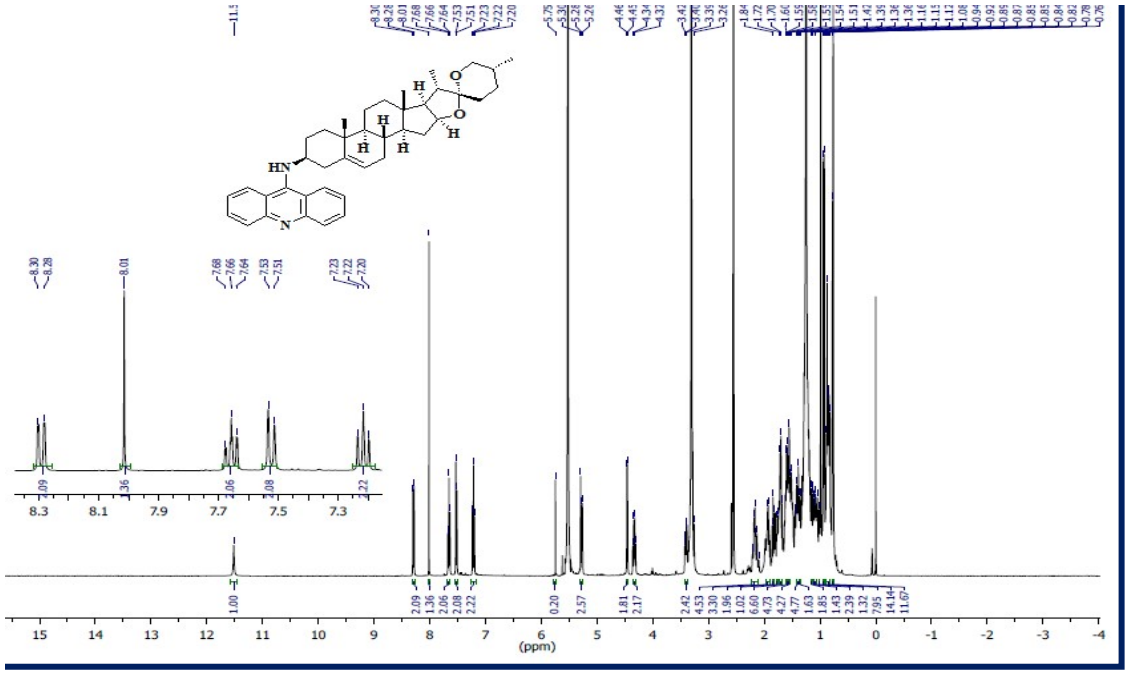

Fig. S16. [1]H NMR spectrum of **D6**

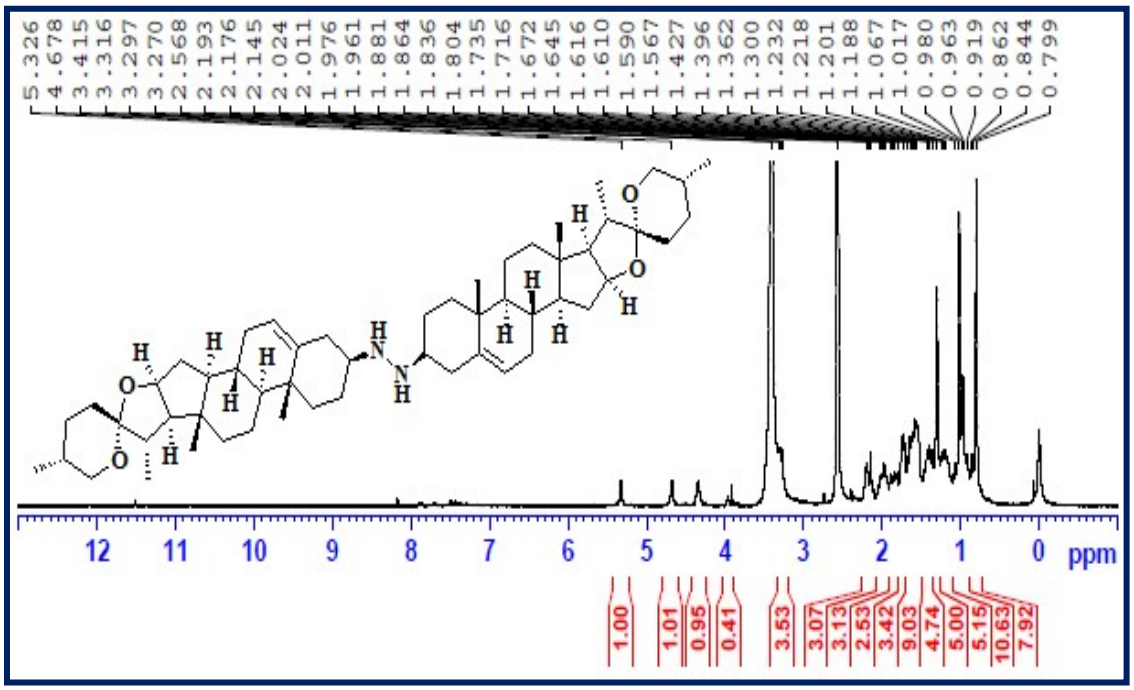

Fig. S17. [1]H NMR spectrum of **D7**

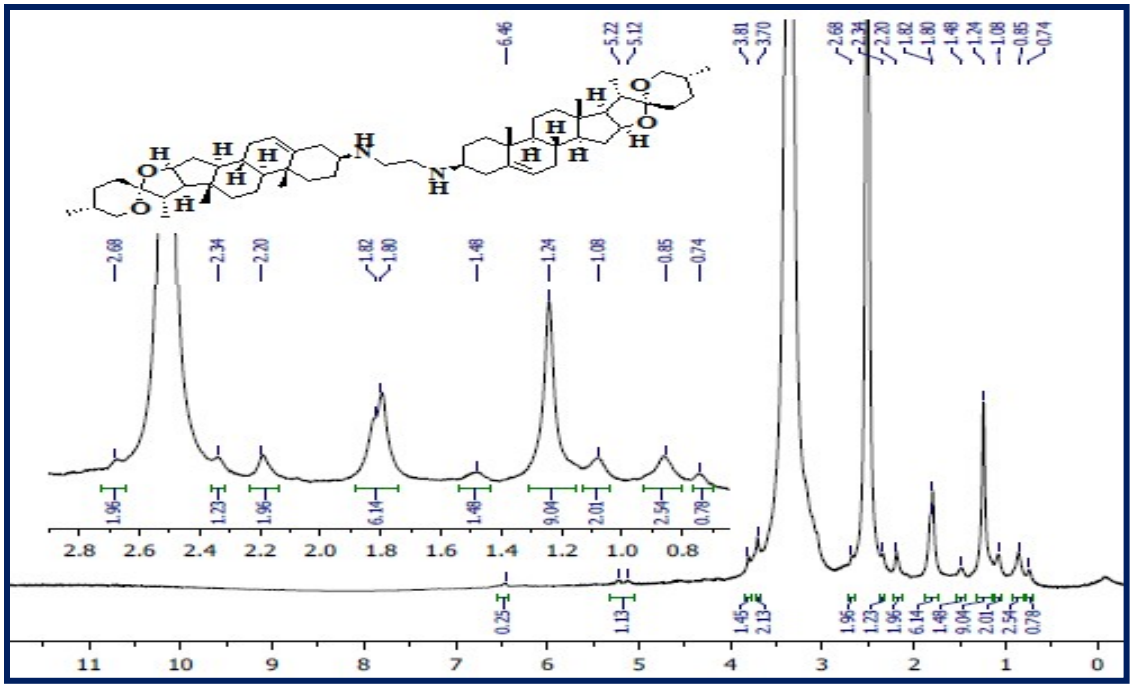

Fig. S18. ^{1}H NMR spectrum of **D8**

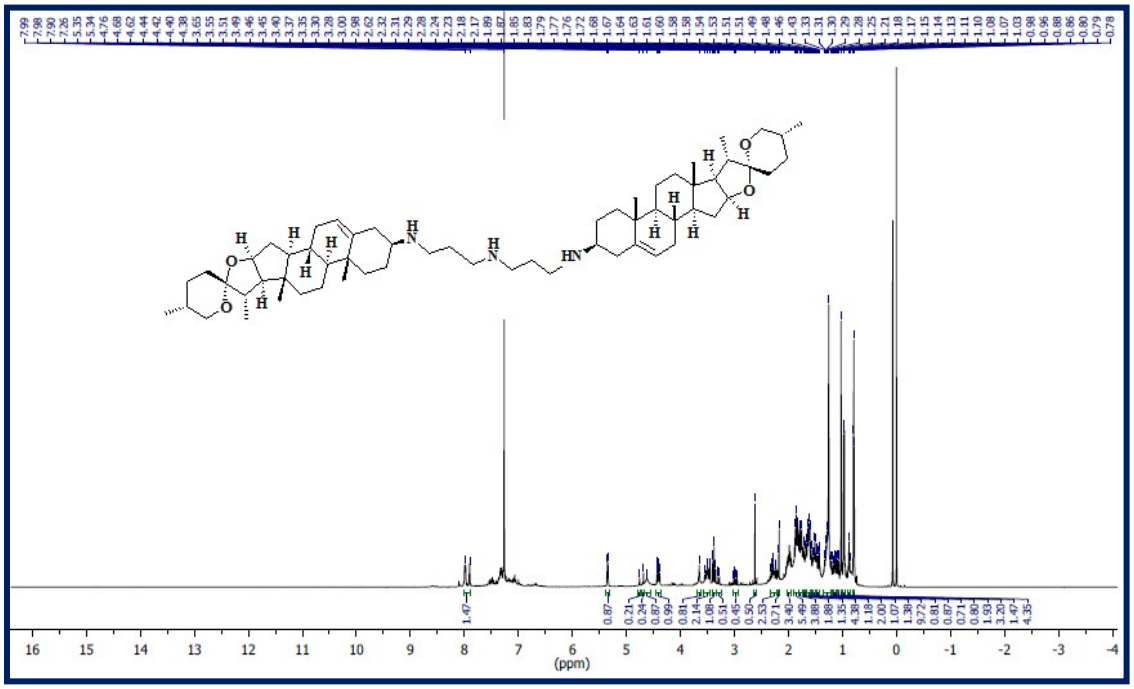

Fig. S19. ^{1}H NMR spectrum of **D9**

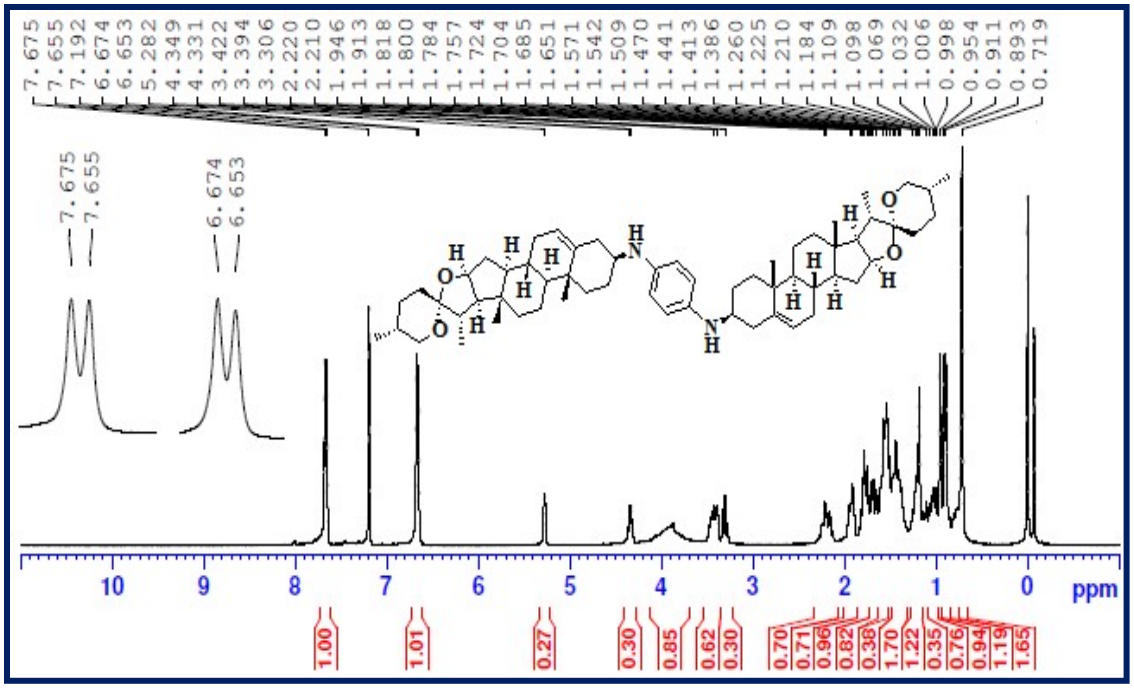

Fig. S20. ^{1}H NMR spectrum of **D10**

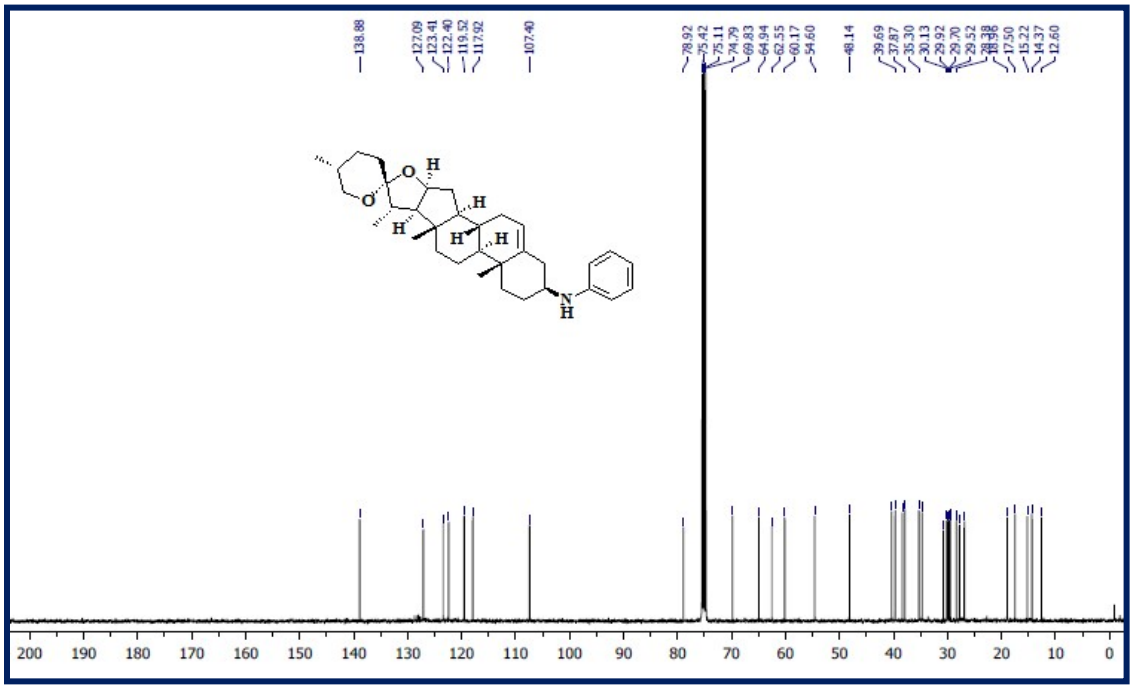

Fig. S21. ^{13}C NMR spectrum of **D1**

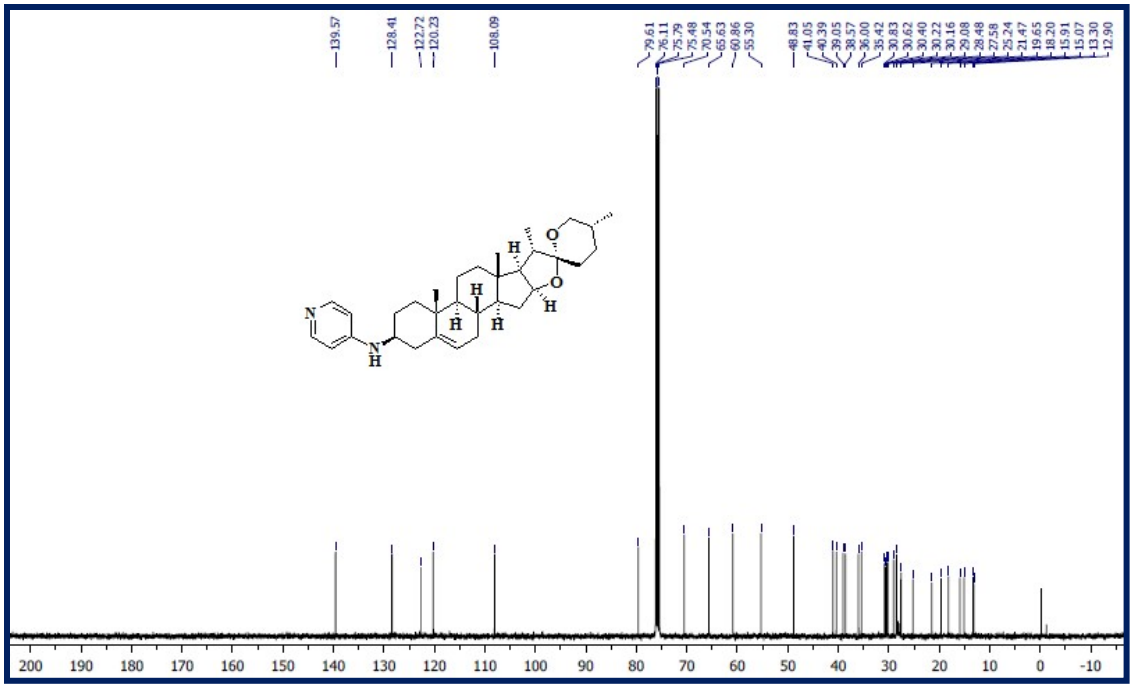

Fig. S22. ^{13}C NMR spectrum of **D2**

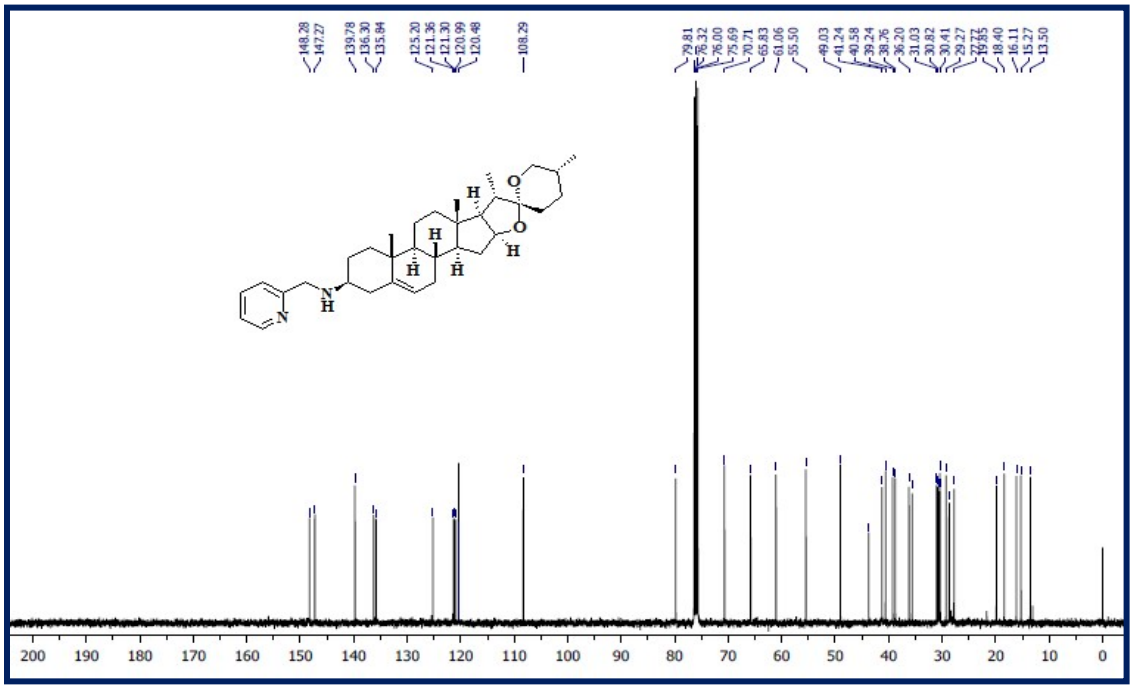

Fig. S23. ^{13}C NMR spectrum of **D3**

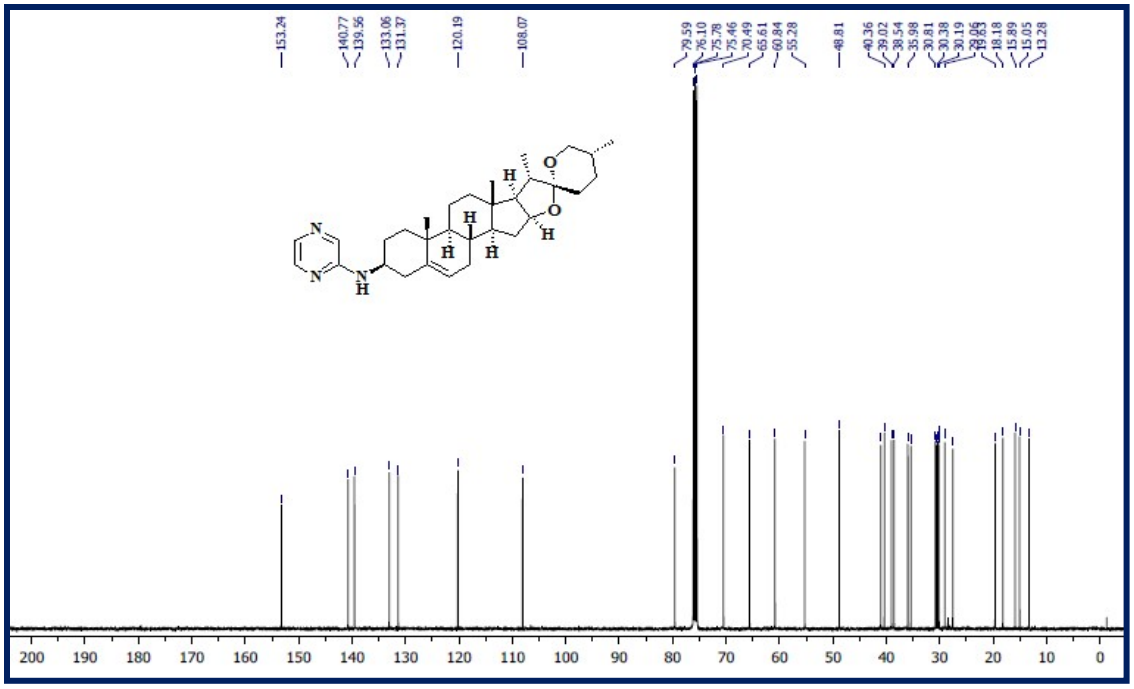

Fig. S24. ^{13}C NMR spectrum of **D4**

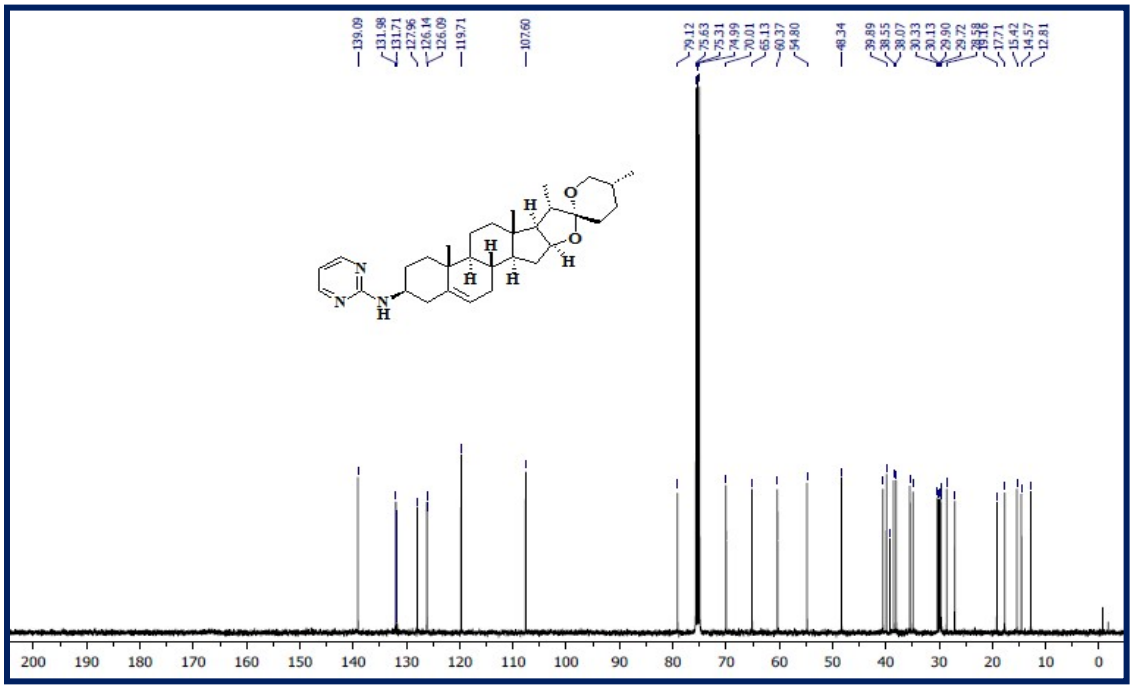

Fig. S25. ^{13}C NMR spectrum of **D5**

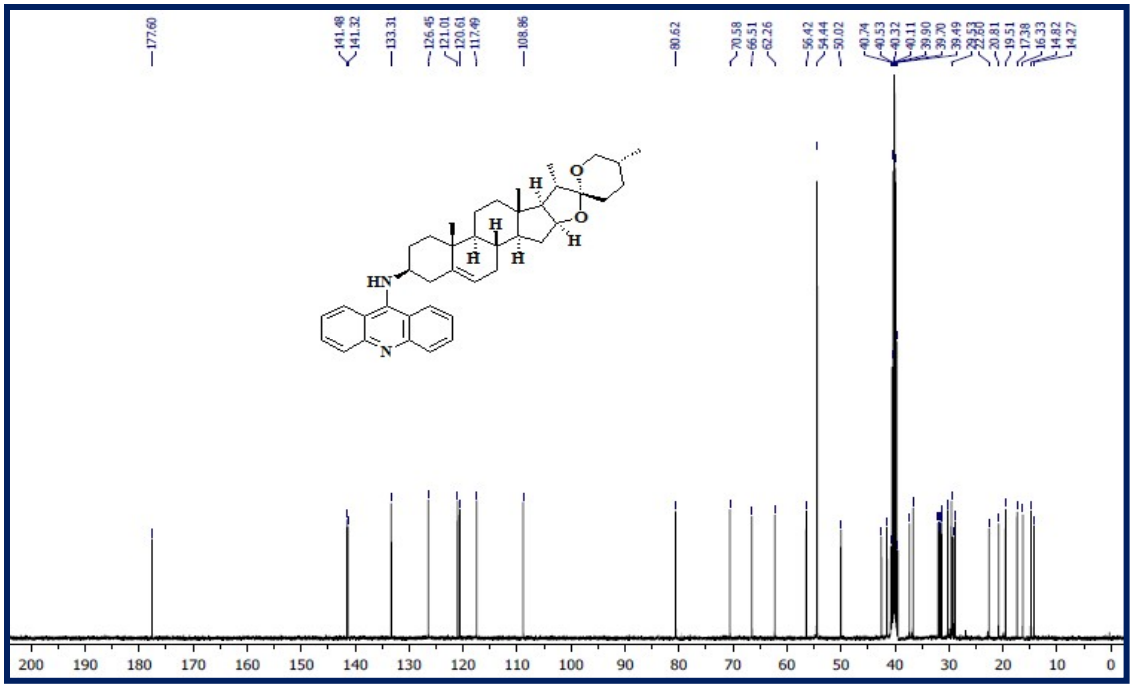

Fig. S26. ^{13}C NMR spectrum of **D6**

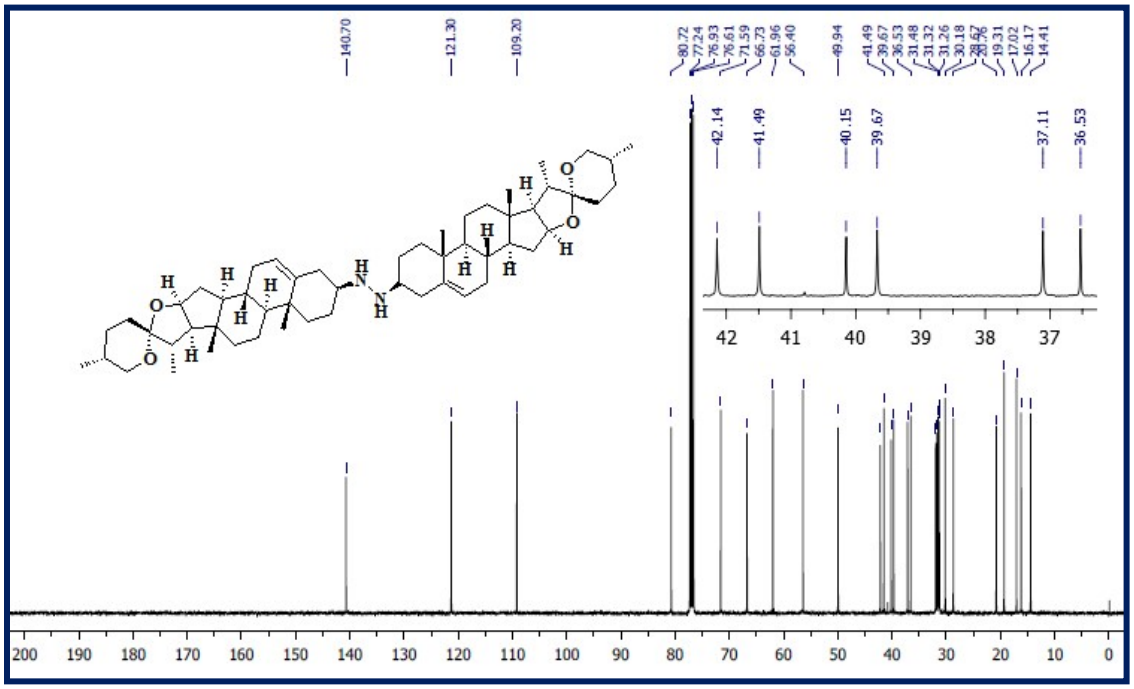

Fig. S27. ^{13}C NMR spectrum of **D7**

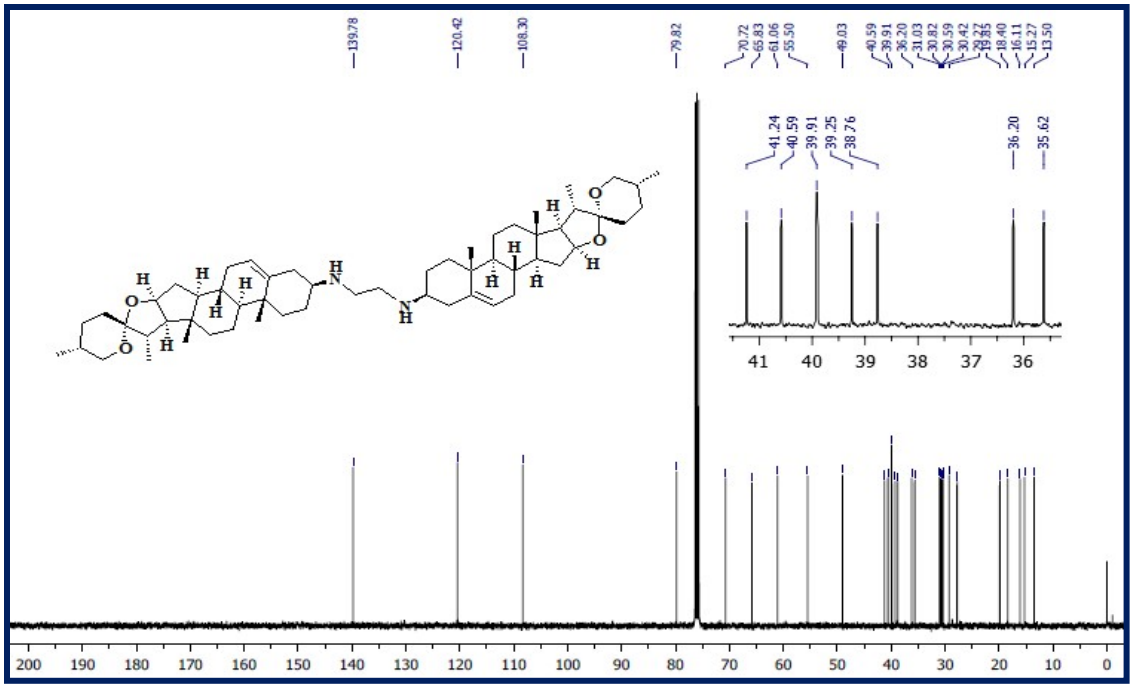

Fig. S28. ^{13}C NMR spectrum of **D8**

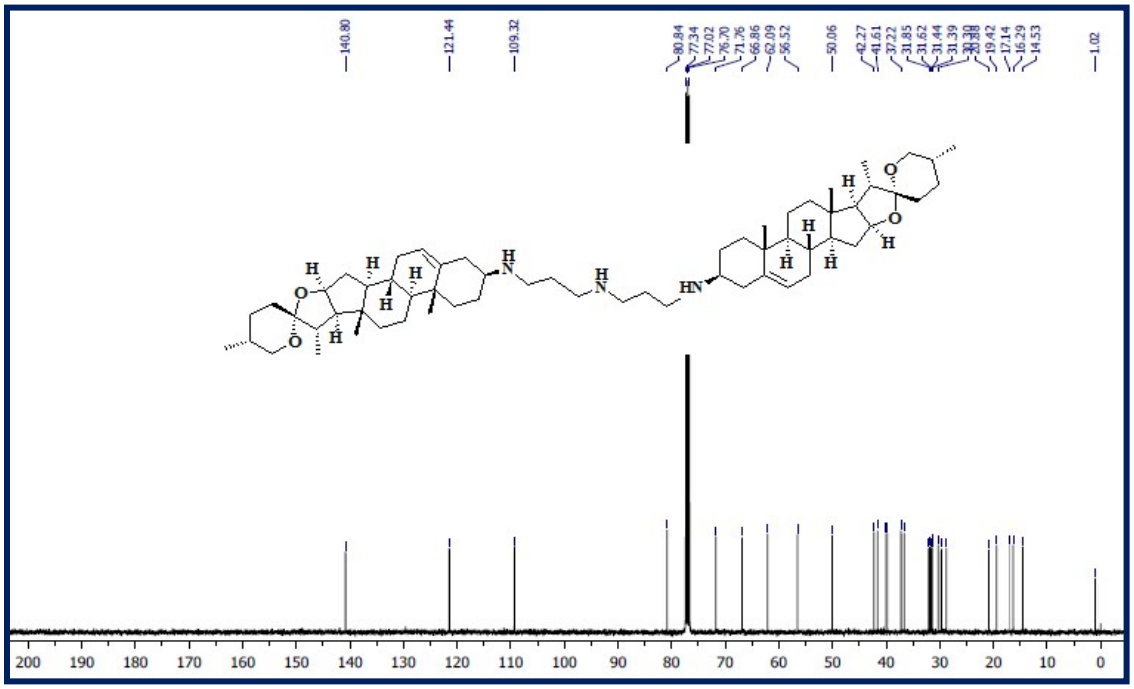

Fig. S29. ^{13}C NMR spectrum of **D9**

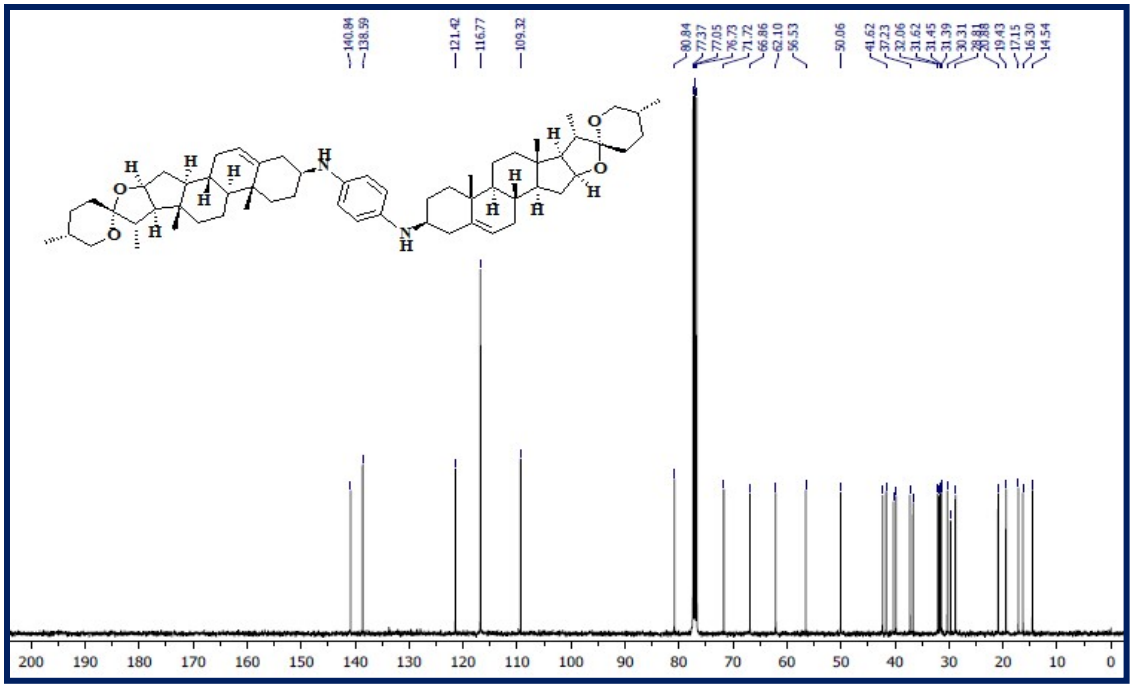

Fig. S30. ^{13}C NMR spectrum of **D10**

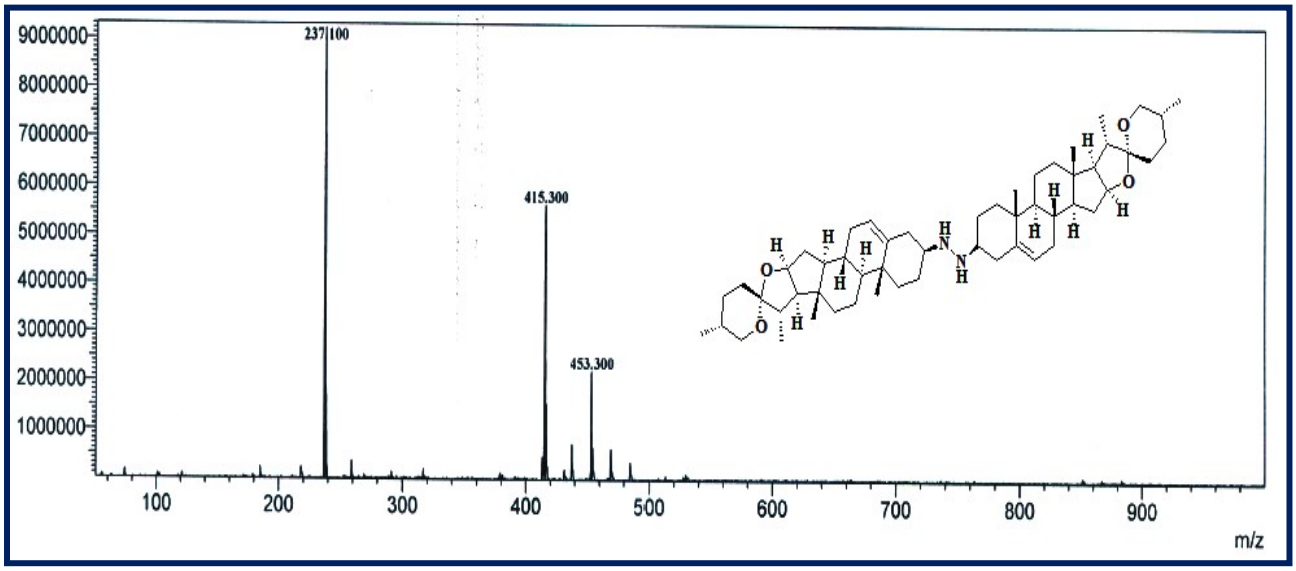

Fig. S31. LCMS spectrum of **D6**

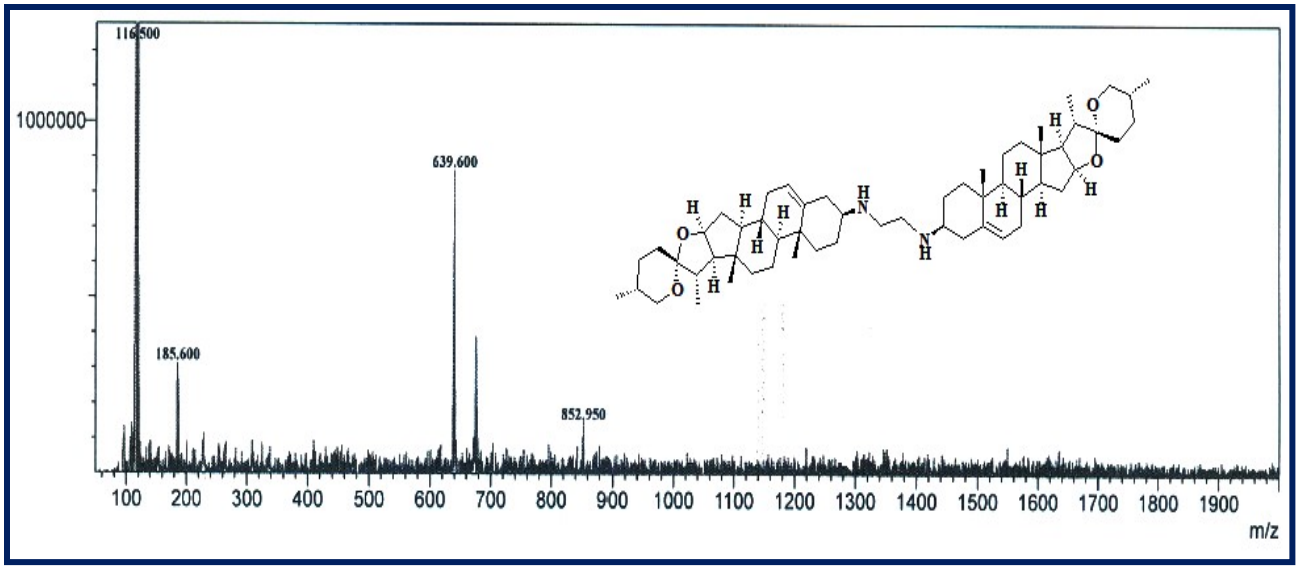

Fig. S32. LCMS spectrum of **D7**

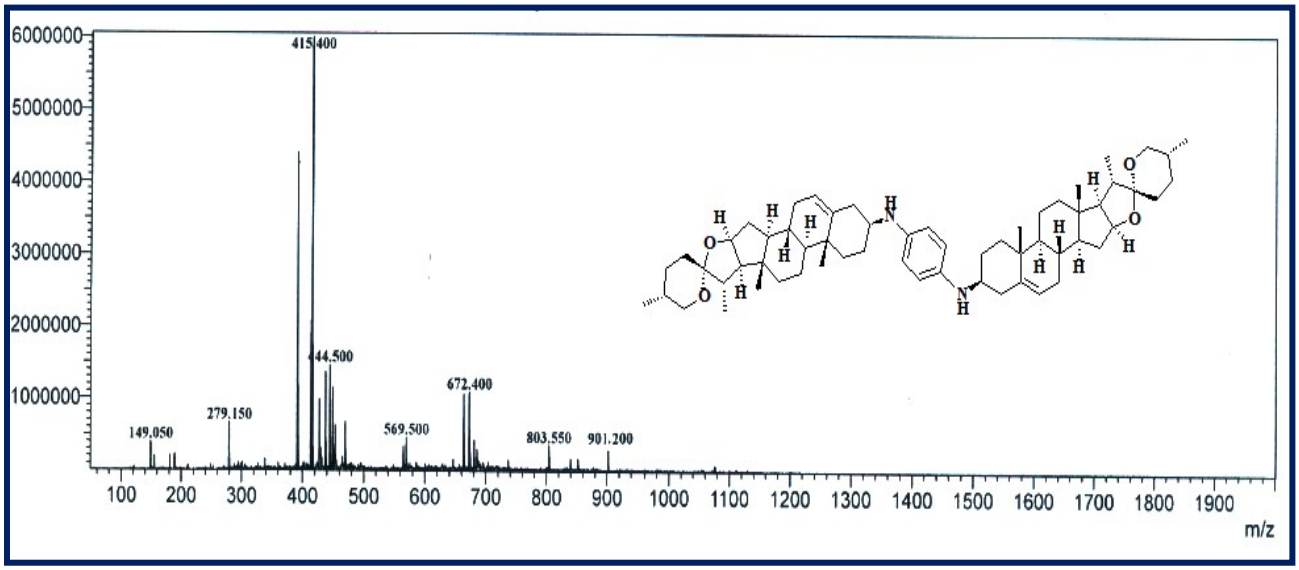

Fig. S33. LCMS spectrum of **D10**

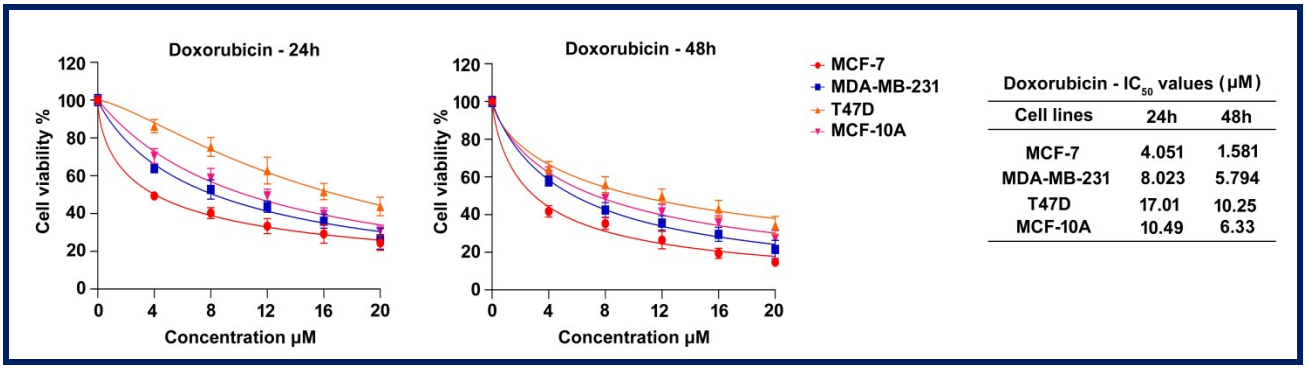

Doxorubicin - IC_{50} values (µM)

Cell lines	24h	48h
MCF-7	4.051	1.581
MDA-MB-231	8.023	5.794
T47D	17.01	10.25
MCF-10A	10.49	6.33

Fig. S34. Activity of doxorubicin on breast cancer cells for an incubation period of 24 and 48 h.

References

S1. A. I. Vogel, Textbook of Practical Organic Chemistry, 5th ed., Longman, London, 1989, 268.

S2. Y. Guo, K. Fhayli, S. Li, Y. Yang, A. Mashat and N. M. Khashab, *RSC Adv*., 2013, **3**, 17693-17695.

S3. S. Selvamurugan, R. Ramachandran, P. Vijayan, R. Manikandan, G. Prakash, P. Viswanathamurthi, K. Velmurugan, R. Nandhakumar and A. Endo, *Polyhedron*, 2016, **107**, 57-67.

S4. M. Muralisankar, S. Sujith, N. S. P. Bhuvanesh and A. Sreekanth, *Polyhedron*, 2016, **118**, 103-117.

S5. Y. Li, Z. Y. Yang and J. C. Wu, *Eur. J. Med. Chem*., 2010, **45**, 5692-5701.

S6. G. Kalaiarasi, Ruchi Jain, H. Puschmann, S. Poorna Chandrika, K. Preethi and R. Prabhakaran, *New J. Chem*., 2017, **41**, 2543-2560.

S7. M. Muralisankar, J. Haribabu, N. S. P. Bhuvanesh, R. Karvembu and A. Sreekanth, *Inorg. Chim. Acta*, 2016, **449**, 82-95.

S8. P. Vijayan, P. Viswanathamurthi, K. Velmurugan, R. Nandhakumar, M. D. Balakumaran, P. T. Kalaichelvan and J. C. Malecki, *RSC Adv*., 2015, **5**, 103321-103342.

S9. B. S. Creaven, M. Devereux, D. Karcz, A. Kellett, M. McCann, A. Noble and M. Walsh, *J. Inorg. Biochem*., 2009, **103**, 1196-1203.

S10. M. Muthu Tamizh, B. F. T. Cooper, C. L. B. Macdonald and R. Karvembu, *Inorg. Chim. Acta*, 2013, **394**, 391-400.

S11. G. Kalaiarasi, S. Rex Jeya Rajkumar, S. Dharani, V. M. Lynch and R. Prabhakaran, *Inorg. Chim. Acta*, 2018, **471**, 759-776.

S12. P. Kalaivani, R. Prabhakaran, F. Dallemer, E. Vaishnavi, P. Poornima, V. Vijaya Padma, R. Renganathan and K. Natarajan, *J. Organomet. Chem*., 2014, **762**, 67-80.

S13. A. Castineiras, N. F. Hermida, I. G. Santos and G. Rodriguez, *Dalton Trans*., 2012, **41**, 13486-13495.

S14. G. Kalaiarasi, S. Dharani, V. M. Lynch and R. Prabhakaran, *Dalton Trans*., 2019, **48**, 12496-12511.

S15. P. Kalaivani, R. Prabhakaran, F. Dallemer, P. Poornima, E. Vaishnavi, E. Ramachandran, V. Vijaya Padma, R. Renganathan and K. Natarajan, *Metallomics*, 2012, **4**, 101-113.

S16. S. Dharani, G. Kalaiarasi, D. Sindhuja, V. M. Lynch, R. Shankar, R. Karvembu and R. Prabhakaran, *Inorg. Chem*., 2019, **58**, 8045-8055.